Achromatic Catadioptric Microscope Objective in Deep Ultraviolet with Long Working Distance

Pei Huang[a,1] and Dietrich Leibfried[b]

[a] Ball Aerospace & Technologies Corp., 1600 Commerce St., Boulder, CO 80301, USA
[b] National Institute of Standards and Technology, 325 Broadway, Boulder, CO 80303, USA

ABSTRACT

We present a microscope imaging optics system that is suitable for simultaneously detecting two species of electrically trapped atomic ions for quantum information processing. The proposed 10x objective features all-spherical surfaces in a catadioptric modification of the Schwarzschild two-mirror configuration and is achromatic at 313 and 280 nm, the two wavelengths of the laser-induced fluorescence from $^9Be^+$ and $^{24}Mg^+$. To correct for aberrations from the fused-silica vacuum window, we use a zero-power doublet made of a positive calcium fluoride and a negative fused-silica meniscus to form an air-gapped Steinheil doublet facing the object. As a result, diffraction limited images are obtained for both wavelengths at a numerical aperture (NA) of 0.5 and a field of view (FOV) of 0.1 mm in diameter. The long working distance (> focal length) of this objective allows imaging of the ions through the vacuum window.

Keywords: Optical design, Microscopy, UV radiation, Catadioptric optics.

1. INTRODUCTION

Deep ultraviolet (DUV) radiation at wavelengths of about 300 nm or shorter has many applications including lithographic processing, surface inspection, environmental monitoring, diagnostics of plasmas, and fluorescence microscopy. For example, in standard lithographic processes, refractive systems made of dozens of lens elements are used to generate diffraction-limited images of photomasks over approximately one-nanometer wavelength bandwidth. This narrow-band achromatic performance is needed to utilize DUV laser power distributed over a broadened linewidth. Recently, a collection of two-species atomic ions (e.g., $^9Be^+$ and $^{24}Mg^+$) electrically trapped in ultrahigh vacuum has been employed to carry out fundamental physics research and quantum information processing[1,2]. Manipulation and readout of atomic quantum states are achieved through laser-induced fluorescence over two narrow lines at 313 and 280 nm for $^9Be^+$ and $^{24}Mg^+$ respectively. Previous designs of refractive imaging optics suffer from large chromatically induced focal shifts and aberrations. The new imaging optics for the two-species experiments must be achromatic at the two widely separated laser lines with large NA and diffraction-limited performance in order to resolve individual atoms that line up within several micrometers of each other. Furthermore, due to the vacuum chamber and fused silica window the working distance must be greater than about 40 mm, and window-induced aberrations must be corrected. Existing diffraction-limited designs either suffer from excessive chromatic dispersion, or have working distances much shorter than the effective focal length (EFL) of the objective.

Prior refractive systems of widely achromatic imaging optics in DUV are typically quite complex, with a large number of elements, and are limited in both the highest achievable NA and performance[3]. This approach is limited fundamentally by the lack of suitable glasses and crystals with high transmittance and low birefringence in DUV. The two commonly used materials in DUV designs are calcium fluoride crystal (CaF_2) and UV-grade fused silica (SiO_2), both of which have negligible transmission losses and birefringence in the wavelength range of interest here. Their refractive properties are listed in Table 1, with CaF_2 and fused silica serving the roles of crown and flint glasses respectively. Exploiting differences in their indices and dispersion, we can cancel the first-order chromatic focal shift in a refractive doublet lens. This doublet configuration serves as a refractive front-end corrector in the optimized catadioptric design discussed in detail in later sections. Recently, a few novel DUV glasses have been incorporated in refractive achromats[4], but their applications are limited due to lack of commercial availability and some undesirable properties of these glasses. Because of the high manufacturing cost and throughput impact associated with complex

---

[1] Email: phuang@ball.com; phone: 1-303-939-6860; fax: 1-303-939-5550.

refractive systems, we conclude that the most sensible approach is to employ inherently achromatic reflective elements for this ion-imaging application.

Table1. Refractive properties of calcium fluoride and fused silica in DUV.

	Calcium fluoride (crown-like)	Fused silica (flint-like)
Index n_{296} at wavelength of 296 nm	1.45481	1.48895
Abbe number $V = (n_{296}-1)/ (n_{280} - n_{313})$	68.19	49.99

Typical high-performance reflective optical systems have one or more aspherical surfaces for controlling aberrations. For DUV optics, these aspherical mirrors must be polished to a high degree of figure accuracy and to very smooth finish because of the short wavelength involved. In addition to the fabrication challenge, alignment of aspherical mirrors is more difficult in that both axis decenter and tilt must be precisely corrected at the same time. These are some of the reasons that we choose the near-concentric concave-convex spherical configuration first proposed as a telescope design by Schwarzschild[5] and later adopted as microscope objectives[6-10]. Besides having all spherical surfaces, the main advantages of the Schwarzschild configuration are its high object-space NA, long working distances, and correction of third-order spherical and coma aberrations. Various forms of catadioptric designs based on the Schwarzschild configuration have been proposed to further increase NA and FOV, and to correct for higher-order aberrations [10-15]. Some of these designs employ many refractive elements and are therefore cost-prohibitive to fabricate and difficult to mount and align. The other drawback of the prior catadioptric forms is that the refractive correctors are typically aplanats positioned very close to the object, and therefore don't allow for a long working distance. Recently, a special form of catadioptric objectives using Mangin mirrors has been suggested for achromatic imaging applications[17,18]. However, some aberrations such as spherochromatism are not sufficiently corrected in this design form.

In this paper, we present an imaging optics system consisting of an objective and relay (tube) optics that satisfies all the requirements for the quantum information processing application. As the initial starting configuration during the optimization, we use a simplified version of Grey's design[13]. The optimized objective optics is a catadioptric modification of the Schwarzschild telescope (42 mm EFL, 0.5 NA) forming a real image at the field stop with a -10x magnification. In order to achieve large NA and to correct window-induced chromatic focal shift and spherical aberrations, the objective uses a positive meniscus of CaF_2 and a negative meniscus of fused silica as an air-spaced Steinheil doublet facing the object. This zero-power doublet is followed by a concave-convex mirror pair in the near-concentric Schwarzschild configuration with about 30% areal obscuration. Most of the optical focusing power is provided by the reflective mirrors, while the refractive doublet serves to correct various aberrations. For ease of mounting and alignment, the convex mirror is physically cemented to the backside of the fused-silica lens. No optical surfaces in the system experience double light passage, so fabrication tolerances can be relaxed. Stray light from scattered excitation laser beams are effectively blocked by the field-stop aperture at the intermediate image. Because of the precise centering of the field-stop aperture in the optical housing and the 10x magnification, offset between the object and axis of the imaging optics can be limited to less than 50 μm. This assures a relatively narrow FOV in the object space over which the objective performance is optimized. After the field stop, a spherical concave mirror relays the intermediate image onto the detector array with additional -12x in lateral magnification. The image quality at both fluorescence wavelengths is limited by the diffraction pattern of the obscured aperture, resulting in a spatial resolution of better than 2 μm in the object space.

2. REQUIREMENTS FOR IMAGING TWO-SPECIES IONS

Since the 1970s, atomic ion particles have been isolated, trapped, and cooled to cryogenic temperatures in electrical and electromagnetic traps inside ultra-high vacuum chambers for studying fundamental physics and developing quantum information processors[1,2]. When these ions are sufficiently cold, they form crystalline structures balancing their Coulomb repulsion with the trapping force. For quantum information processing, the typical number of ions in the crystal is less than ten with a size of a few tens of micrometers. Cooling, detection, and quantum-state manipulation of these trapped ions are carried out through interactions with focused beams of stabilized, narrow-linewidth tunable lasers. Here, a particular ion can be resonantly excited from a ground state into the designated higher energy state, from which it then decays back to the ground state due to quantum selection rules giving off a randomly distributed fluorescence photon.

This excitation-decay process is called a cycling transition and can be repeated many times to be detected by the imaging optics to form an integrated image. The axis of imaging optics is generally not collinear with the excitation laser beam, typically at $\geq 45^o$, in order to suppress directly scattered laser light from vacuum windows and the trap structure. The objective optics must have a long working distance in order to accommodate a vacuum chamber structure, and the window-induced aberrations must also be corrected for in the design. In addition, an intermediate real image is typically needed so that a field stop can be installed to further reduce the amount of stray light. Large object space NA is needed in order to maximize collection efficiency and increase spatial resolution.

The presence of two ion species with two widely separated fluorescence lines (e.g., 313 nm for $^9Be^+$ and 280 nm for $^{24}Mg^+$) presents unique challenges for the objective design. First, the chromatic focal shift must be well corrected at these two wavelengths due to the short depth of field from the large object-space NA. Second, spherical aberrations and associated spherochromatism from the vacuum window must also be compensated for at both wavelengths. Finally, coma aberrations should be controlled. Because the FOV is relatively small, astigmatism, field curvature, distortion, and lateral color are negligible. Since ion crystal images are recorded by an analog position-sensing resistive cathode with coarse spatial resolution (~ 100 μm), a relatively large lateral magnification is needed. The photo cathode has a front-end image intensifier that has good responsivity at both 313 and 280 nm.

Table 2. Requirements of imaging optics for two-species ion experiments.

Wavelengths	Dual laser lines at 280.0 & 313.0 nm
Object space NA	≥ 0.5
Object field of view diameter	0.1 mm
Object space resolution	≤ 2.0 μm
Magnification	$\approx 120x$
Working distance	≥ 40 mm
Vacuum window	Corrected for 2 mm thick fused silica
Optical surfaces	Prefer all spherical
Transmission efficiency	$\geq 50\%$
Linear obscuration ratio	≤ 0.6 (throughput and diffraction MTF)
Areal obscuration ratio	≤ 0.4
Coatings	AR ≥ 0.99 transmission; HR ≥ 0.98 reflection.
Inter. image & field stop	Yes
Ambient temperature change	$\pm 1°C$
Total track length	≤ 1.5 m
Wavefront error	Diffraction limited at both wavelengths

Table 2 summarizes of requirements for the imaging optics system including both the objective and relay optics. Object NA target is a compromise between high collection efficiency and size of optics as determined by the working distance. Spatial resolution in the object space is determined mainly by the smallest lattice gap size of the ion crystals. One drawback of the Schwarzschild configuration is that there is necessarily significant obscuration by the convex secondary mirror for large NA and magnification ratio. For this application, however, the amount of throughput loss from obscuration is tolerable provided that high-performance anti-reflection (AR) and high-reflection (HR) coatings are used for the refractive and reflective surfaces. We use custom-designed dual-band AR and HR coatings to minimize Fresnel losses because the fluorescence signal is well concentrated in the two narrow bands of the excitation lasers. Since the imaging optics is situated in a well-controlled laboratory environment, crystalline materials having large coefficient of thermal expansion (CTE) such as CaF_2 can be used in the design. A relatively long track length can be accommodated as long as it fits on the stable optical bench. Finally, because of the degraded diffraction limit from the aperture obscuration[19] and expected low contrast from the detector, the wavefront error must be quite small in order to meet the spatial resolution requirement.

Table 3. Top level design parameters for the objective and relay optics.

	Objective	Relay
Optical design	Catadioptric Schwarzschild	Concave spherical mirror
Magnification	-10x	-12x
Focal length (mm)	41.8	50.0
Diameter (mm)	≤ 110 (4.3")	≤ 12.5
Linear obscuration	0.55	0
Wavefront error	Diff. Limited	Diff. limited
Field of view diameter (mm)	0.1	1.0

We use a UV-grade high-quality stock spherical concave mirror and a flat fold mirror as relay optics. Furthermore, for maximum flexibility and robustness, we want both the objective and relay optics to have diffraction-limited performance separately rather than correcting the imaging system as a whole. This requires that the objective optics must have a large enough lateral magnification to achieve a small NA after the intermediate image and field stop. Table 3 shows top-level properties of the objective and relay optics with their respective assigned magnifications. With the 10x magnification ratio of the objective, 0.05 NA beam in the intermediate image space stays close to being diffraction limited through the additional 12x magnification by the spherical relay mirror. To steer the relayed beam away to the detector, a 45° fold mirror with a center through hole is inserted near the intermediate image plane. By locating the fold mirror near the intermediate image, the mirror mount structure can also support the field stop, and the size of the clear hole is minimized so that no additional beam clipping results. The total optical track length is about 1.2 m from the object to the detector.
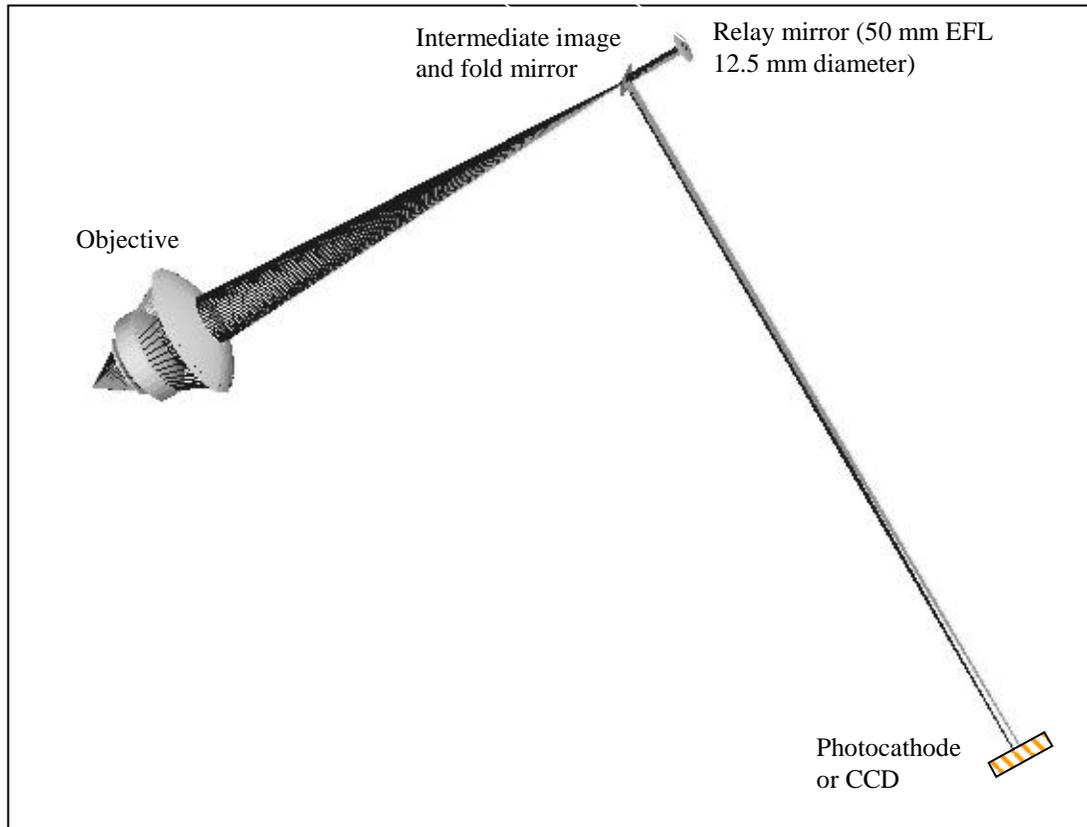

Figure 1. Imaging optics systems layout with the catadioptric objective and spherical relay mirror.

3. OPTIMIZED CATADIOPTRIC OBJECTIVE

In this section, we discuss the optimization process and detailed features of the optimized catadioptric objective design. We follow the traditional convention of going from the long conjugate (magnified intermediate image) to the short conjugate (object) in designing the objective optics. The starting point of the optimization process is the well-known Schwarzschild concentric two-mirror telescope for the infinite conjugate case. Optimizing this configuration for the finite conjugate at 10x magnification with the vacuum window and fixing the working distance, we find that the dominant wavefront errors come from higher-order spherical aberrations and spherochromatism. Next, we try to improve the design by inserting a weakly focusing calcium-fluoride singlet between the Schwarzschild telescope and the short conjugate. The higher-order spherical aberrations have decreased somewhat, but the spherochromatism has not diminished significantly while first-order chromatic focal shift is introduced. Finally, we insert another fused-silica lens between the Schwarzschild telescope and the CaF_2 lens to obtain a highly corrected wavefront for the optimized design. The system aperture stop has been fixed at the convex secondary mirror to minimize obscuration ratio. We have also utilized the Hammer global optimization algorithm to verify that the optimized design is close to the global optimum of this configuration class.
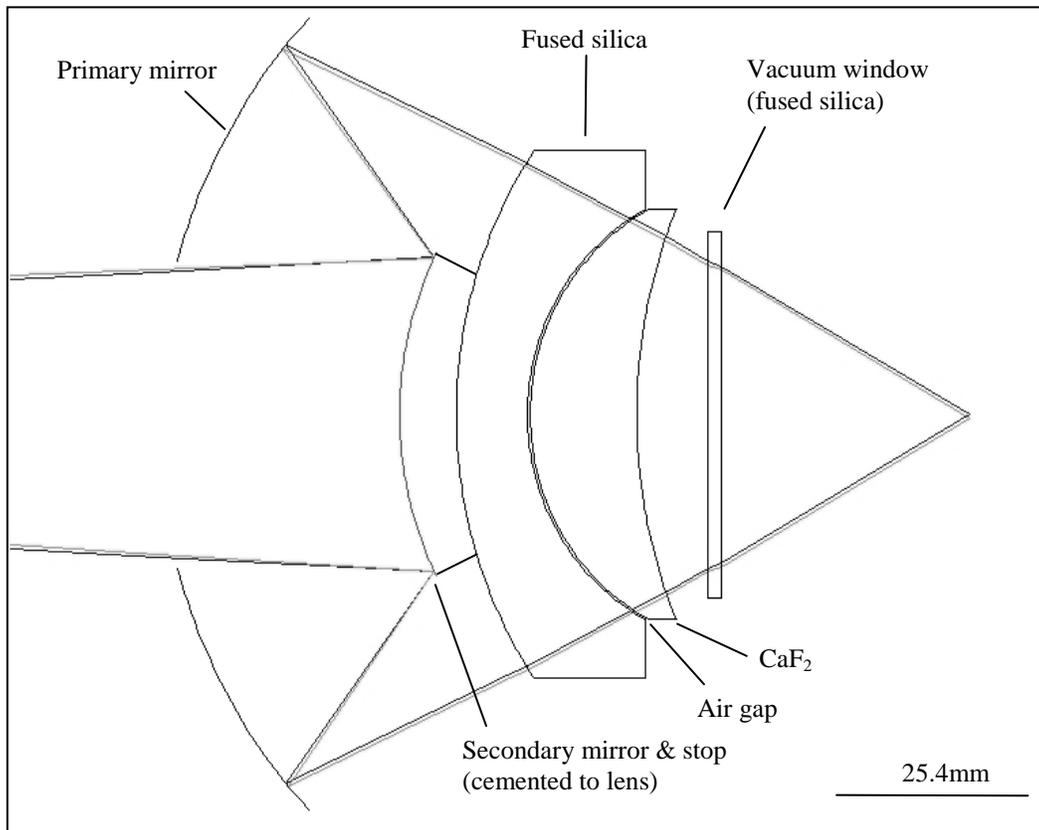

Figure 2. Optimized catadioptric design form of the achromatic microscope objective.

The two-dimensional cross section of the optimized objective optics is shown in Figure 2, with an exaggerated 10x FOV for clarity. Going from right to left, fluorescence light from the two ion species first goes through the vacuum window and then the air-gapped Steinheil doublet made of positive CaF_2 and negative SiO_2 meniscus elements. The focusing power of the doublet corrector is quite weak, with an effective focal length of about 900 mm. The main purpose of the refractive corrector is to cancel spherical aberrations and chromatic focal shift and spherochromatism from the vacuum window at the two design wavelengths. For convenience in mounting and alignment, the convex secondary mirror is cemented to the back surface of the negative fused-silica meniscus lens. Using a layer of black paint and with DUV absorbing optical cement, the interface serves as the controlled obscuration so that no unintended ghosts can co-exist

with the main image. The conditioned beam is then projected to the intermediate real image by the concave-convex reflective mirrors through the clear hole in the concave primary mirror. After being filtered by the field-stop aperture, the intermediate image is relayed by the stock concave mirror and steered by the fold mirror to the detector at the final image plane (see Figure 1).

Detailed optical description data of the optimized objective are listed in Table 4 in the sequence of the long to short conjugates. Note that the primary mirror has a diameter of about 108 mm (4.25 inch) with a focal length of 39.4 mm. For a mirror of spherical surface, this focusing speed is not difficult to achieve in the fabrication. The difference in radii of curvature (29.317 mm) between the primary and secondary mirrors is somewhat shorter than their separation (34.212 mm) to accommodate the finite 10x conjugate image. For the doublet refractive corrector, we use a narrow air gap rather than a cemented interface because most optical cements or epoxies absorb light or degrade over time in the DUV region. In addition, a cemented doublet may have stress problem because of the large mismatch in CTE between CaF_2 and fused silica. The radius of curvature of the fused-silica lens facing the narrow air gap is slightly longer than that of the CaF_2 lens, ensuring that their edges remain untouched in the mechanical mounting structure.

Table 4. Prescription of optimized all-spherical design of the achromatic objective (dimensions are in mm).

Surface	Comment	Radius of curvature	Thickness	Glass	Diameter
1	Inter. Image	Infinity	422.689		
2	Secondary	49.487	-34.212	MIRROR	44.0
3	Primary	78.804	42.212	MIRROR	108.0
4	Negative lens	64.741	10.000	F_SILICA	72.0
5		31.895	0.432		54.0
6	Positive lens	31.834	15.000	CAF2	54.0
7		72.771	9.955		54.0
8	Vac. Window	Infinity	2.000	F_SILICA	50.0
9		Infinity	35.000		50.0
10	Object	Infinity	0.000		

Detailed performance data in the object space of the optimized catadioptric objective are presented in Figure 3. The spot diagrams for 313 and 280 nm at center and edge field positions in Figure 3(a) show very tight geometrical ray foci, indicating highly corrected axial color, all orders of spherical aberrations, and spherochromatism. Diffraction-limited Airy disks for the obscuration-free aperture at 313 nm are drawn as a reference. Wavefront optical path difference fan plots in Figure 3(b) demonstrate that the nominal design has peak-to-valley errors much smaller than 1/20 wave (scale of the plots) for both wavelengths and is therefore very much diffraction limited. For the edge of the FOV, a small amount of coma aberration is visible. Since the central part of the wavefront is blocked by the obscuration of the secondary mirror, smaller peak-to-valley error results than indicated by the curves.

As we mentioned earlier, the main drawback of this design is the impacts from the obscuration of the secondary mirror. Besides reducing the system's signal power throughput, the obscuration introduces additional diffraction effects absent for systems with a clear circular aperture. As a result, the diffraction-limited modulated transfer function (MTF) degrades at small spatial frequencies and enhances at large spatial frequencies. Predicted MTFs of the optimized objective design are shown in Figure 3(c) in comparison to the diffraction limit from the obscured aperture. Because of the high degree of aberration correction, the predicted MTFs are virtually indistinguishable from the diffraction limit for both wavelengths over the entire FOV. At a modulation frequency of 500 cycles/mm corresponding to the 2 μm spatial resolution, the reduced MTF is about 0.5, therefore still providing enough contrast to satisfy the required resolving power in the object space.

The predicted chromatic focal shift over the wavelength range between 313 and 280 nm is plotted in Figure 3(d). This result clearly shows the achromatic performance at the two laser-induced fluorescence lines of interest in this application. Two features of the optimized objective design provide the precise cancellation of first-order chromatic focal shift at the two wavelengths: first, the reflective Schwarzschild configuration is inherently wavelength independent; second, the two elements of the Steinheil doublet have their respective focusing powers according to the

achromatization rule such that the combined focal length is the same at the two wavelengths of interest. Note that since secondary axial color aberration is not generally correctable with a doublet lens, large focal shift results for the wavelength region between 313 and 280 nm. An apochromatic triplet will be needed to achieve correction of the secondary axial color, but this is difficult to achieve at a DUV wavelength due to lack of suitable glasses with proper dispersion characteristics. For this application, however, achromatic performance at two wavelengths is adequate.

We estimate the power throughput of the entire imaging system in Table 5 (going from object to the intermediate image) based on the assumption that custom AR and HR coatings covering dual wavelength bands will be applied to the refractive and reflective surfaces, respectively. For the AR coating, 0.99 transmission efficiency is attainable for both wavelengths and polarizations over the range of angle of incidence. For HR, we assume that 0.98 reflectivity is the minimum near both 0° and 45° angles of incidence. The major contribution to the power-loss budget comes of course from the areal obscuration of 0.3 in the objective optics. This ratio can be reduced somewhat at the expense of large primary mirror diameter and increased wavefront errors. Absorptions in the window and doublet corrector are insignificant at both wavelengths. The estimated final system throughput is about 61%. This figure is comparable to the existing monochromatic refractive lens system, which operates at a smaller NA and with more refractive elements.
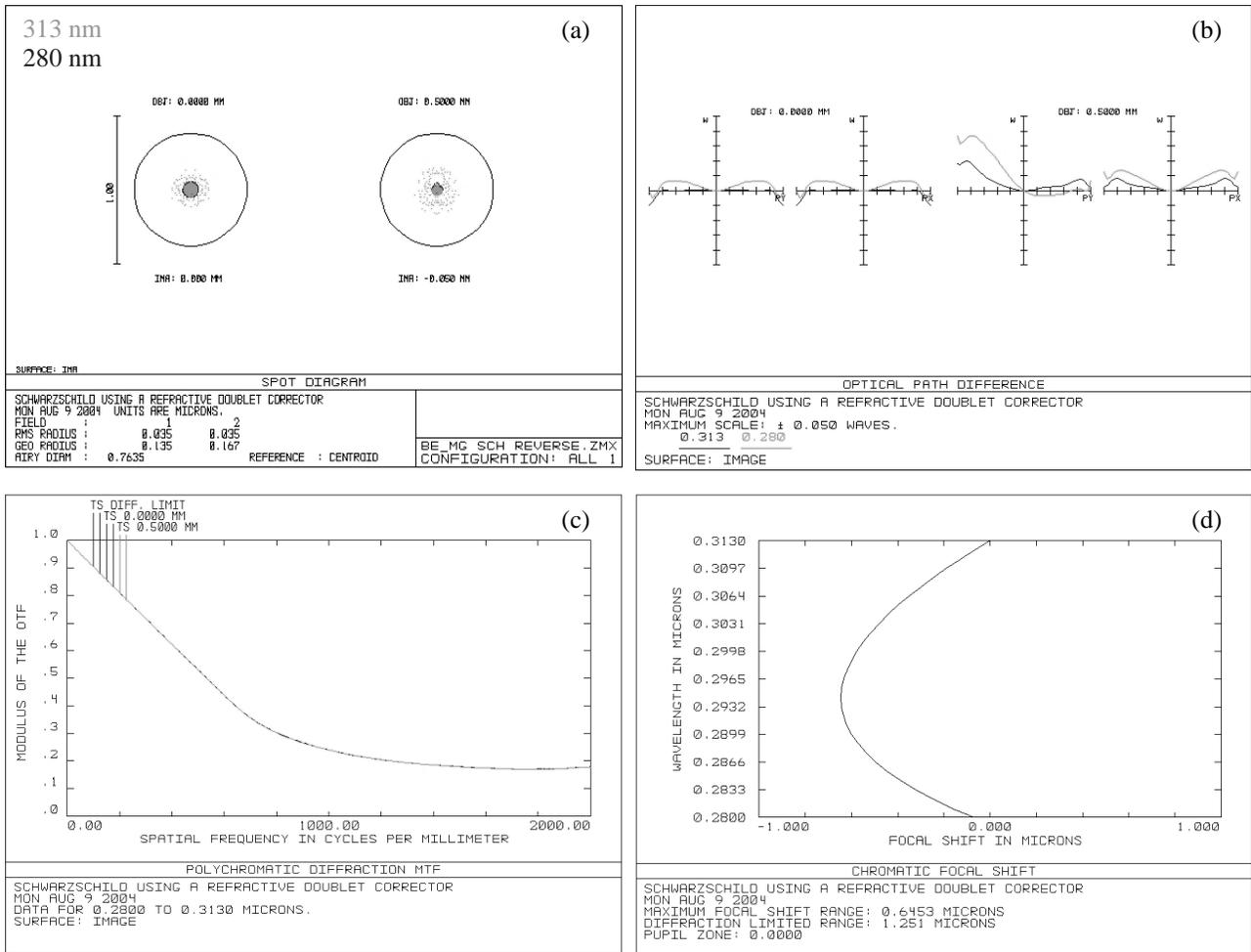

Figure 3. Predicted performance of the optimized catadioptric objective in the object space: (a) Two-wavelength spot diagrams for center and edge of FOV. (b) Two-wavelength OPD fan diagrams for center and edge of FOV. (c) Two-wavelength diffraction modulated transfer functions for center and edge of FOV in comparison to the diffraction limit. (d) Chromatic focal shift.

Table 5. Estimated imaging system throughput transmission efficiency.

	At 313 nm	At 280 nm
Fused-silica window (2 mm)	0.98	0.98
CaF$_2$ meniscus (15 mm)	0.98	0.98
Fused-silica meniscus (10 mm)	0.98	0.98
Obscuration	0.70	0.70
Primary mirror	0.98	0.98
Secondary mirror	0.98	0.98
Relay mirror	0.98	0.98
Fold mirror	0.98	0.98
Total	0.61	0.61

Fabrication tolerances for the optical elements are relatively stringent for irregular deviations from spheres due to the short wavelength in the DUV. However, the targeted irregularity figures are well within range for state-of-art optical polishing shops. Tolerances for surface radius of curvature and lens thickness are relatively loose provided that active in-situ alignment is performed during the assembly of the objective. Specifically, we plan to assemble and align the doublet corrector with the cemented secondary mirror first to form a front-end subassembly. The precise alignment of this triplet subassembly follows standard techniques. For the final alignment of the front-end subassembly to the primary mirror, we plan to adjust the relative x-y-z positions of the subassembly with guidance from an interferometer.

4. SUMMARY AND DISCUSSIONS

In conclusion, we have briefly reviewed prior microscope objective designs in the DUV region and have discussed the requirements for imaging two-species ions for quantum information processing. We have proposed a new imaging optical system based on a catadioptric modification of the Schwarzschild telescope and shown that it can satisfy all the requirements and be manufactured at low cost and with high quality. The optimized objective design is achromatic at 313 and 280 nm wavelengths, and is highly corrected for aberrations affecting the image quality.

Further simplification of the proposed imaging optics is possible. For example, the two surfaces facing the air gap in the doublet can have the same radius of curvature, so that a direct optical contact mount can be applied, eliminating two glass-air interfaces. The induced wavefront error from this simplification is relatively small. Additionally, the 45° fold mirror can be replaced with one at approximately 5° angle of incidence. This will eliminate the need of using two difference types of HR coatings and therefore reduce manufacturing cost and increase reflectance performance.

ACKNOWLEDGEMENTS

REFERENCES

1. See for example, D. Leibfried, et al., *Toward Heisenberg-Limited Spectroscopy with Multiparticle Entangled States,* Science **304**, 1476 (2004), and references therein.
2. M.D. Barrett, et al., *Sympathetic Cooling of $^9Be^+$ and $^{24}Mg^+$ for Quantum Logic,* Phys. Rev. A **68**, 042302-1 (2003).
3. See for example, N. Yamada, et al., *Achromatic Lens for Ultraviolet Rays,* U.S. patent #5,028,967, (1991).
4. K-H. Schuster, *Achromatic Lens System for Ultraviolet Radiation with Germanium Dioxide Glass,* U.S. patent #6,064,516, (2000).
5. K. Schwarzschild, *Theorie der Spiegeltelescope*, Astr. Mitt. Koenigl. Sternwarte Goettingen, (1905).
6. A. Bouwers, *Achievements in Optics,* Sec.1.5, Elsevier (1946).
7. C.R. Burch, *Reflecting Microscopes*, Proc. Phys. Soc. **59**, 41 (1947).
8. C.R. Burch, *Semi-aplanat Reflecting Microscopes*, Proc. Phys. Soc. **59**, 47 (1947).

9. P. Erdos, *Mirror Anastigmat with Two Concentric Spherical Surfaces,* JOSA **49**, 877 (1959).
10. W. Smith, *Modern Optical Engineering, Third Ed.,* Chapter 13, McGraw-Hill (2000).
11. D.S. Grey, *A New Series of Microscope Objectives: I & II,* JOSA **39**, 719 (1949).
12. D.S. Grey, *Optical System,* U.S. patent #2,520,633, (1950).
13. D.S. Grey, *Catadioptric Optical System,* U.S. patent #2,576,011, (1951).
14. D.S. Grey, *Reflecting Mirror Optical Objective,* U.S. patent #2,684,015, (1954).
15. M. Laikin, *Lens Design,* Chapter 11, Marcel Dekker, (1995).
16. D.R. Shafer, Y-H. Chuang, and B-M.B. Tsai, *Broad Spectrum Ultraviolet Catadioptric Imaging System,* U.S. patent #5,717,518, (1998).
17. J.E. Webb, C.T. Tienvieri, *Double Mirror Catadioptric Objective Lens System with Three Optical Surface Multifunction Component,* U.S. patent #6,560,039 B1, (2003).
18. W. Smith, *Teaching an Old Mirror New Tricks,* SPIE OE Magazine, 28 (June, 2003).
19. H.F.A. Tschunko, *Imaging Performance of Annular Apertures,* Appl. Opt. **13**, 1820 (1974).